energies

MDPI

Article

Quasi-Wireless Capacitive Power Transfer for Wire-Free Robotic Joints †

Tyler Marcrum [1,2], John-Caleb Williams [2,3], Christopher S. Johnson [2,3], Matthew Pearce [4], Carson Pope [1,2], C. W. Van Neste [2,3,*], Charles Vaughan [5] and Darren Boyd [5]

[1] Center for Energy Systems Research, Tennessee Tech University, 1020 Stadium Dr., Cookeville, TN 38505, USA; tgmarcrum42@tntech.edu (T.M.); cdpope42@tntech.edu (C.P.)
[2] AETHR Laboratory, Tennessee Tech University, 1020 Stadium Dr., Cookeville, TN 38505, USA; jawilliams46@tntech.edu (J.-C.W.); csjohnson43@tntech.edu (C.S.J.)
[3] Department of Electrical and Computer Engineering, Tennessee Tech University, 115 W. Tenth St., Cookeville, TN 38505, USA
[4] Department of Electrical and Computer Engineering, University of Auckland, 34 Princes Street, Auckland CBD, Auckland 1010, New Zealand; matthew.pearce@auckland.ac.nz
[5] United States National Aeronautics and Space Administration (NASA), Marshall Space Flight Center, Martin Rd SW, Huntsville, AL 35808, USA; charles.m.vaughan@nasa.gov (C.V.); darren.r.boyd@nasa.gov (D.B.)
* Correspondence: cvanneste@tntech.edu
† This paper is an extended version of our paper published in 2023 IEEE Wireless Power Technology Conference and Expo (WPTCE), San Diego, CA, USA, 4–8 June 2023.

Abstract: Robotics is a highly active, multidisciplinary research area with a broad list of applications. A large research focus is to enhance modularity in order to expand kinematic capabilities, lower fabrication time, and reduce construction costs. Traditional wiring within a robot presents major challenges with mobility and long-term maintenance. Designing robotics without wires would make a significant functional impact. This work presents a new application of quasi-wireless capacitive power transfer that investigates impedance matching parameters over a highly resonant, coupled transmission line to achieve efficient power transfer over a robotic chassis. A prototype is developed and its operating metrics are analyzed with regard to the matching parameters.

Keywords: quasi-wireless; capacitive; robotics; magnetic; CPT

Citation: Marcrum, T.; Williams, J.-C.; Johnson, C.S.; Pearce, M.; Pope, C.; Van Neste, C.W.; Vaughan, C.; Boyd, D. Quasi-Wireless Capacitive Power Transfer for Wire-Free Robotic Joints. *Energies* **2024**, *17*, 2858. https://doi.org/10.3390/en17122858

Academic Editor: Alon Kuperman

Received: 7 May 2024
Revised: 31 May 2024
Accepted: 4 June 2024
Published: 11 June 2024

1. Introduction

A robust number of wires is the typical solution when constructing a robot. Wiring is problematic and requires maintenance, as a single break can result in system failure, or worse a hazardous environment. Wireless Power Transfer (WPT) could be a possible means to remove wiring within robotic design [1–8]. Researchers have investigated Inductive Power Transfer (IPT), demonstrating a 1 degree of freedom experimentally [9], which was theoretically expanded to 3 degrees of freedom [10]. A major challenge with IPT comes from lower misalignment tolerances between the transmitter (Tx) and receiver (Rx). For power transfer within a robotic appendage, developing methods to maintain IPT alignment can be difficult and lead to limitations in motion. Additionally, there is still a bulk of wires and electronics (such as an inverter) that must be present at each linkage if IPT is used [3,11,12]. A second method of WPT that exists is Capacitive Power Transfer (CPT), where an electric field at high frequency is used to transfer power from one electrode "plate" to another. CPT approaches have two primary configuration methodologies: a bipolar method, where the Tx has two physical plates with a matching two plate Rx [13], and a unipolar (or single-wire) method, which consists of a single Tx plate and a ground plane with the Rx either sharing the Tx ground plane or having a capacitive connection to that ground plane through a counterpoise (a large return plate) [14]. For design of a fully

wireless robotic system, the same issues arise that were present in IPT, a need for a bulk of wiring and an inverter between each wireless joint [15–17]. Due to space limitation on most robotic systems, it is generally not possible to include a large counterpoise for single-wire CPT. Therefore, it can be concluded that there is no existing WPT methodology that can remove the wiring completely within a robotic system. Table 1 includes a side-by-side comparison of state-of-the-art WPT techniques, listing the pros and cons. It includes IPT, Magnetic Resonance Power Transfer (MRPT), CPT, and Acoustic Power Transfer (APT).

Table 1. Advantages and disadvantages of various WPT configurations.

	IPT	MRPT	CPT	APT
Pros	Most commonly used WPT technique [18] Capable of high power transmission level (kW) [19] High power transfer efficiency [19,20] Low sensitivity to environmental factors (pollutants and weather) [21]	Employs resonance frequency matching of Tx and Rx, which allows for less reliance on alignment [18,19] Range can be extended using intermediate coils that are tuned to the same system's resonant frequency [22,23]	Transfer power through metallic materials without significant eddy current losses [19,20,22] Less reliance on Tx and Rx alignment [18] Implementation is often more cost efficient than with IPT systems [20]	Most secure WPT methodology due to the safe transmission of sound waves in the required frequency band [21] Resistivity to electromagnetic interference due to the transfer of energy occurring through sound waves [18]
Cons	Potential of significant eddy current losses [19] Potential for cross-talk due to inductance leakage [23] Challenging to transmit power through objects such as walls [21]	Complex systems, potentially consisting of additional matching networks [18] High sensitivity to frequency shifts due to resonance frequency aligned Tx and Rx [18]	Bipolar CPT requires many capacitive plates for transmission [18] Single-Wire CPT requires a large counterpoise [14] Normally, lower transmission efficiency and distance than IPT [18,20]	Relatively low power transmission levels (mW), often being used in bio-medical devices [18] Hardly explored in robotics due to low transmission efficiency [18]

With this in mind, the work presented here aims to create a new method of robotic design that completely removes wiring along and between joints of a robotic chassis. A quasi-wireless capacitive (QWiC) method will be utilized that replaces the large counterpoise requirement of a single-wire CPT system with a small quarter wave resonator (QWR) acting as a Rx, providing a compact method of power transfer over the surface of a robotic chassis. This approach presents a significant deviation from the standard two-wire electrical design methodology, simplifying it to only one electrical connection per joint. In other words, the robot wiring will be completely replaced by a conductive chassis that will allow the QWR and chassis surface to act as a power conduit.

One challenge in utilizing the QWiC method is that the QWR is highly sensitive to external influences very near or touching the QWR receiver. This makes impedance matching significantly more difficult. Firstly, the impedance becomes position dependent, such that the parameters of the matching network are based on the location it is placed (similar to an antenna). Secondly, unlike an antenna and most problematic, when the matching network is connected, the internal coupling at each section of the QWR causes the entirety of the QWR's transmission line characteristics to change, making a simple smith-chart impedance calculation nearly impossible. To address this issue, a less invasive technique will be presented that offers a way to improve the impedance match of the load, without drastically affecting the QWR's transmission line characteristics.

2. Materials and Methods

Conventional IPT and CPT designs require a minimum of two impedance matched Tx and Rx elements with proper alignment to allow for efficient power transfer [24]. Typically, these systems are operated in a frequency range where the currents and voltages are

uniform, allowing a lumped circuit model approach when making impedance matching calculations. However, a QWiC system operates in highly resonant mode where the distributed transmission line inductances at each section are mutually coupled to adjacent sections, forming what was defined as a mutually coupled transmission line (μcT-line) [25].

To reduce the impact of changes in the μcT-line, the approach will be to form "taps" along the QWR. The idea is to shunt more current into the load rather than the QWR using the tap. This form of shunt-based impedance matching attempts to create a parallel path that utilizes a capacitor to negate the effects of load on the QWR operation.

The voltage distribution along an untapped QWR's μcT-Line, with respect to the circuit neutral, is found to be [25]

$$V = Z_T I_S (1 - e^{-\phi}) \tag{1}$$

where I_S is the current flowing through the QWR, Z_T is the total impedance of the QWR that is exponentially distributed by $(1 - e^{-\phi})$, and ϕ is the position along the QWR in radians. This expression is only valid when the QWR's inductance is in resonance with the stray capacitance, which is the condition required to transfer power. The stray capacitance has the most impact at the top, or free end, of the QWR. The bottom of the QWR represents the majority of the distributed inductance. It is expected that Equation (1) will change with an applied tap.

To derive the impact a tap would make on the QWR, Figure 1 is used as the distributed model of the μcT-line with a matching network shunted at the lower end. The total current in the QWR can be split between an upper impedance (Z_{UR}) and a lower impedance (Z_{LR}). Segmenting the QWR into four discrete sections and applying loop analysis produces

$$[\frac{-j}{\omega x_1' C_1} + j\omega x_1 L_1]i_1 + [\frac{j}{\omega x_1' C_1} - \omega x_2 M_{12}]i_2 + [-j\omega x_1 L_1]i_L = V_S, \tag{2}$$

$$[\frac{j}{\omega x_2' C_2} + \omega x_2 M_{21}]i_1 + [\frac{-j}{\omega x_1' C_1} + j\omega x_2 L_2 - \frac{j}{\omega x_2' C_2}]i_2 + [\frac{j}{\omega x_2 C_2} - \omega x_3 M_{23}]i_3 = 0, \tag{3}$$

$$[\frac{j}{\omega x_2' C_2} + \omega x_2 M_{32}]i_2 + [\frac{-j}{\omega x_2' C_2} + j\omega x_3 L_3 - \frac{j}{\omega x_3' C_3}]i_3 + [\frac{j}{\omega x_3' C_3} - \omega x_4 M_{34}]i_4 = 0, \tag{4}$$

$$[\frac{j}{\omega x_3' C_3} + \omega x_3 M_{43}]i_3 + [\frac{-j}{\omega x_3' C_3} + j\omega x_4 L_4 - \frac{j}{\omega x_4' C_4}]i_4 = 0, \tag{5}$$

$$[-j\omega x_1 L_1]i_1 + [-j\omega x_2 M_{12}]i_2 + [R_L' + j\omega L_L - \frac{j}{\omega C_L} + j\omega x_1 L_1]i_L = 0, \tag{6}$$

where R' is the equivalent resistance of the load that accounts for transformation and rectification. Equation (6) can be written in terms of i_L

$$i_L = \frac{x[-j\omega x_1 L_1]i_1 + [-j\omega x_2 M_{12}]i_2}{[R_L' + j(\omega L_L - \frac{1}{\omega C_L} + j\omega x_1 L_1)]} \tag{7}$$

Dividing i_L into its real and imaginary parts yields

$$i_L = \frac{j\omega L_1 x_1 R_L'(I_1) + \omega L_1 x_1(\omega L_L - \frac{1}{\omega C_L}\omega L_1 x_1)(I_1)}{B} + \frac{j\omega x_2 M_{12} R_L'(I_2) + \omega x_2 M_{12}(\omega L_L - \frac{1}{\omega C_L}\omega L_1 x_1)(I_2)}{B} \tag{8}$$

where

$$B = (R_L')^2 + (\omega L_L + \omega L_1 x_1 - \frac{1}{\omega C_L})^2 \tag{9}$$

Substituting Equation (8) into (2), the real and imaginary parts become
Real:

$$\frac{\omega^2 x_1^2 L_1^2 R_L'(I_1)}{B} + \frac{\omega^2 L_1 M_{12} x_1 x_2 R_L'(I_2)}{B} - V_S + \ldots \tag{10}$$

Imaginary:

$$\ldots j(\omega L_1 x_1 - \frac{1}{\omega C_1 x_1'} - \omega^2 \gamma_1) I_1 + j(\frac{1}{\omega C_1 x_1'} + \omega M_{12} x_2 - \omega^2 \gamma_2) I_2 = 0, \tag{11}$$

where

$$\gamma_1 = \frac{L_1^2 x_1^2 (\omega L_L - \frac{1}{\omega C_L} + \omega L_1 x_1)}{B}; \tag{12}$$

$$\gamma_2 = \frac{L_1 M_{12} x_1 x_2 (\omega L_L - \frac{1}{\omega C_L} + \omega L_1 x_1)}{B}. \tag{13}$$

γ_1 is the reactive effect of the tapped load branch current (I_L in Figure 1) on the self inductance of the Lower Resonator, while γ_2 is the effect of I_L on the mutual coupling between Sections 1 and 2. At resonance, the reactive components of the μcT-line will cancel at each distributed section. Following the same procedure presented in [26] but for a tapped system, the reactive terms for each loop can be equated, where the capacitive elements can be used to link the self inductances to the mutual inductances in each equation, Equations (2)–(5). This represents a total resonant condition, which is experimentally observable in the QWR when at resonance. From Equation (11),

$$\omega L_1 x_1 = -\omega M_{12} x_2 + \omega^2 \gamma_1 + \omega^2 \gamma_2. \tag{14}$$

Solving for M_{12},

$$M_{12} = \frac{-L_1 x_1 + \omega \gamma_1 + \omega \gamma_2}{x_2}. \tag{15}$$

Substituting M_{12} into the reactive components of (3),

$$L_2 x_2 + M_{23} x_3 = (\frac{-L_1 x_1 + \omega \gamma_1 + \omega \gamma_2}{x_2}) x_1. \tag{16}$$

Solving for M_{23},

$$M_{23} = \frac{-L_2 x_2^2 - L_1 x_1^2 + \omega \gamma_1 x_1 + \omega \gamma_2 x_1}{x_2 x_3}. \tag{17}$$

Substituting M_{23} into the reactive parts of (4),

$$L_3 x_3 + M_{34} x_4 = M_{23} x_2 = \frac{-L_2 x_2^2 - L_1 x_1^2 + \omega \gamma_1 X_1 + \omega \gamma_2 x_1}{x_3}. \tag{18}$$

Solving for M_{34},

$$M_{34} = \frac{-L_1 x_1^2 - L_2 x_2^2 - L_3 x_3^2 + \omega \gamma_1 x_1 + \omega \gamma_2 x_1}{x_3 x_4}. \tag{19}$$

Finally, substituting M_{34} into the reactive parts of (5),

$$\omega L_4 x_4 - \omega (\frac{-L_1 x_1^2 - L_2 x_2^2 - L_3 x_3^2 + \omega \gamma_1 x_1 + \omega \gamma_2 x_1}{x_4}) = \frac{1}{\omega C_4 x_4}. \tag{20}$$

Rearranging

$$\omega^2 (L_1 x_1^2 + L_2 x_2^2 + L_3 x_3^2 + L_4 x_4^2) - \omega^3 \gamma_1 x_1 - \omega^3 \gamma_2 x_1 = \frac{1}{C_4} \tag{21}$$

Equation (21) is similar to what is found in [26] but with additional γ terms that subtract from the total additive inductance. Using the same procedure to derive Equation (21),

the capacitive terms can be solved and equated to Equation (21). This yields an expression for the resonant condition of the QWR.

$$\frac{(x_1+x_2)}{\omega C_1 x_1'}+\frac{(x_2+x_3)}{\omega C_2 x_2'}+\frac{(x_3+x_4)}{\omega C_3 x_3'}+\frac{1}{\omega C_4}=\omega(L_1x_1^2+L_2x_2^2+L_3x_3^2+L_4x_4^2)-\omega^2 x_1\gamma_1 \quad (22)$$

Note that the γ_2 terms cancel in Equation (22). From Equation (22), it can be seen that at resonance, γ_1 acts to subtract the inductance of the QWR below the tap location (x_1 section). This causes the non-linear distributions of the μcT-line to start at the tap location and not at the connection of the supply. This is an important result, as it shows that the non-linear effects of the μcT-line have been greatly decoupled from the load branch, such that variations in the load and associated matching network will not greatly change the electrical length of the QWR once connected. When $X_C = X_L$, the most current will flow through the load branch, improving the efficiency of transmission.

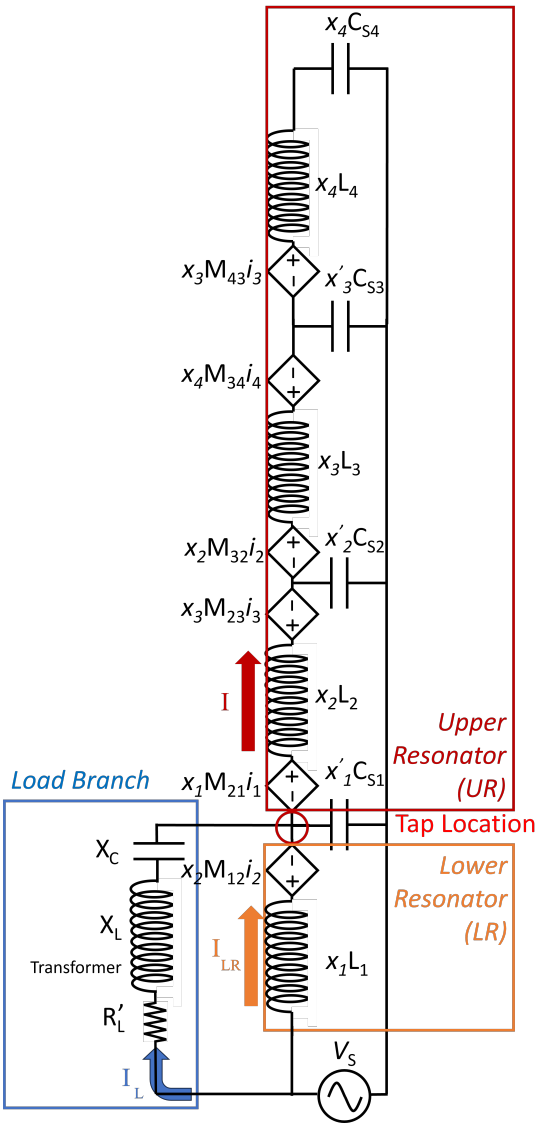

Figure 1. The new addition of a capacitance in series to the transformer and in parallel to the μcT-line seen in [25].

The current of the QWR can be approximated by assuming that the non-linear voltage distribution occurs only in the upper portion of the QWR, above the tap, allowing the portion below the tap to be a paralleled equivalent of Z_{LR} and Z_L.

$$I_{QWR} \approx \frac{V_S}{\frac{Z_{LR}+Z_L}{Z_L Z_{LR}} + Z_{UR}(1 - e^{-\Phi})} \tag{23}$$

It is important to validate the above theory. The current along the QWR is difficult to directly measure since probes placed very near the QWR will alter the stray capacitance, drastically changing the parameters of the μcT-line. Using thermal imaging, it is possible to approximate the distribution of current in the system. Referring to Figure 2, the heat in the image is from the i^2R losses in the QWR; by plotting the thermal distribution from the image, the square root of this thermal distribution yields an approximate current along the QWR. The measured input current (I) was used to properly scale the data extracted from the thermal image. The predicted versus experimental measurements are shown in Figure 3, where the predicted current was plotted from Equation (23). The plots are in decent agreement but are not exact since the thermal distribution is not a direct, one-to-one measurement of current—only an approximation. Thermal conduction within the copper windings of the QWR will spread with time. This causes error when trying to approximate the value of current from the thermal image.

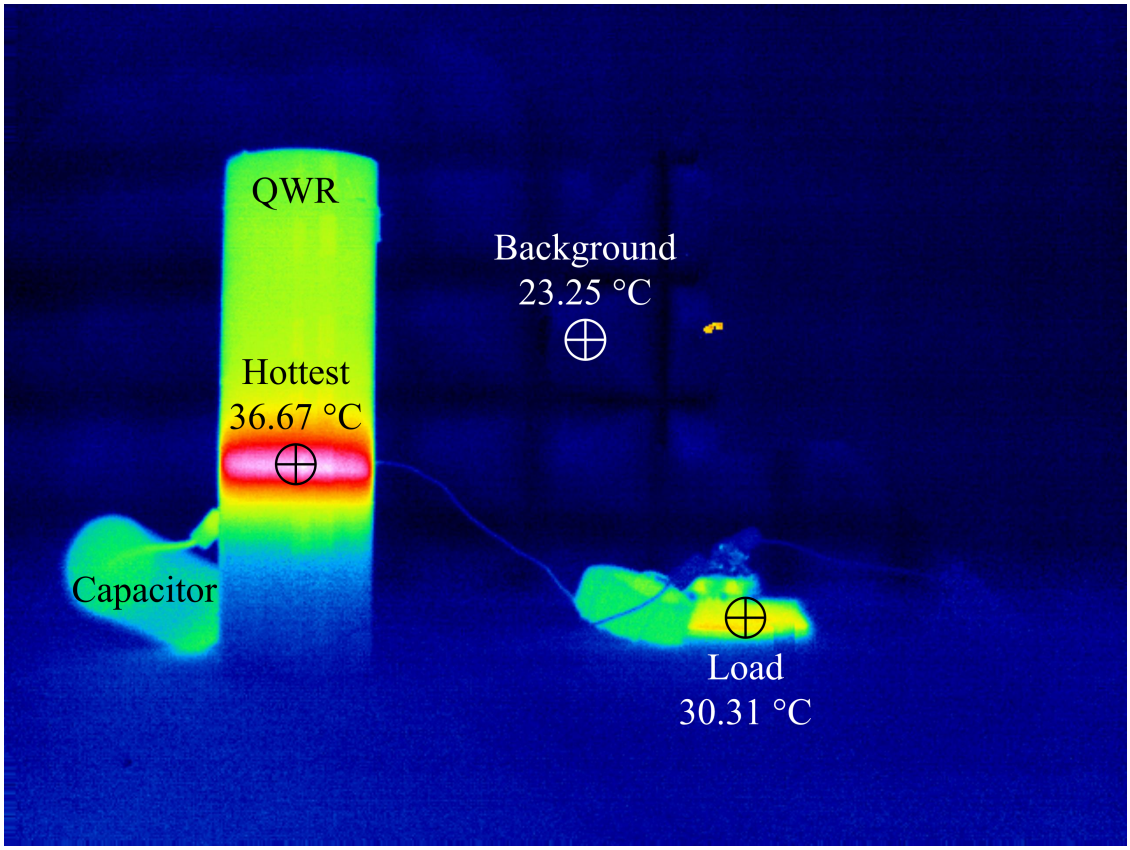

Figure 2. Thermal imagery of the QWR with a parallel load along the transmission line. This has the concentration of current at the tap location rather than the bottom of the coil.

2.1. Experimental Setup

A 1-degree of freedom prototype was fabricated and is shown in Figure 4. The prototype consisted of a motor with an encoder, a QWR, a frame, and a concentric base plate. The frame was 3-D (Drawn using Autodesk Inventor Professoinal 2021 Build:421 and printed using Original Prusa i3 MK3S) printed using Polylactic acid (PLA) filament, which was then coated with conductive paint (841AR Super Shield Nickel Conductive Paint). Permanent magnets were attached to the bottom of the frame such that the the prototype would magnetically connect to the base plate. The base plate comprised an acrylic sheet that housed two electrodes: a steel "anode" plate and a grounded steel "cathode"

plate. RF power was supplied to the center section of the base plate via a coaxial cable. Nylon M3 screws were used to secure the electrodes to the acrylic plate. Due to the high impedance operation of the QWR, a ferrite toroidal transform was used in the matching branch Figure 4a, while also providing isolation for the load. The matching transformer was composed of 20 gauge magnet wire and a Fair-Rite type 67 core. The toroid had an outer diameter of 35 mm, inner diameter of 22.5 mm, and a thickness of 13 mm Figure 5. The overall circuit is shown in Figure 4a, where the QWR was constructed of 176 turns of 22 gauge magnet wire with a total physical length of 135 mm and an outer diameter of 47.5 mm. Taps were placed every 15 turns along the entirety of the QWR.

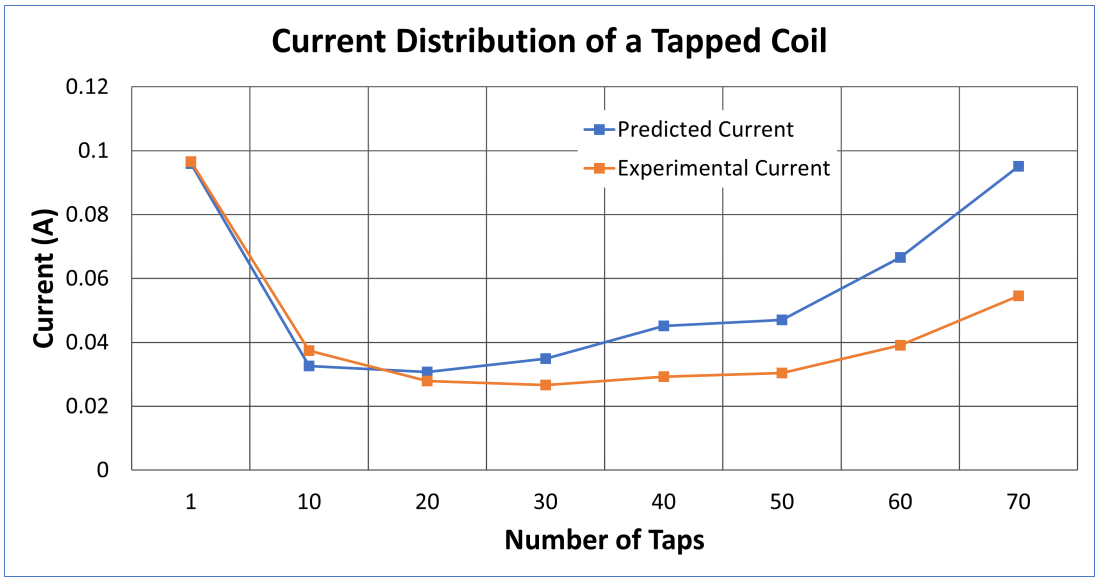

Figure 3. The theory compared to the experimental current distribution of a tapped coil. Equation (6) was used to find the theoretical current with the values calculated per turn.

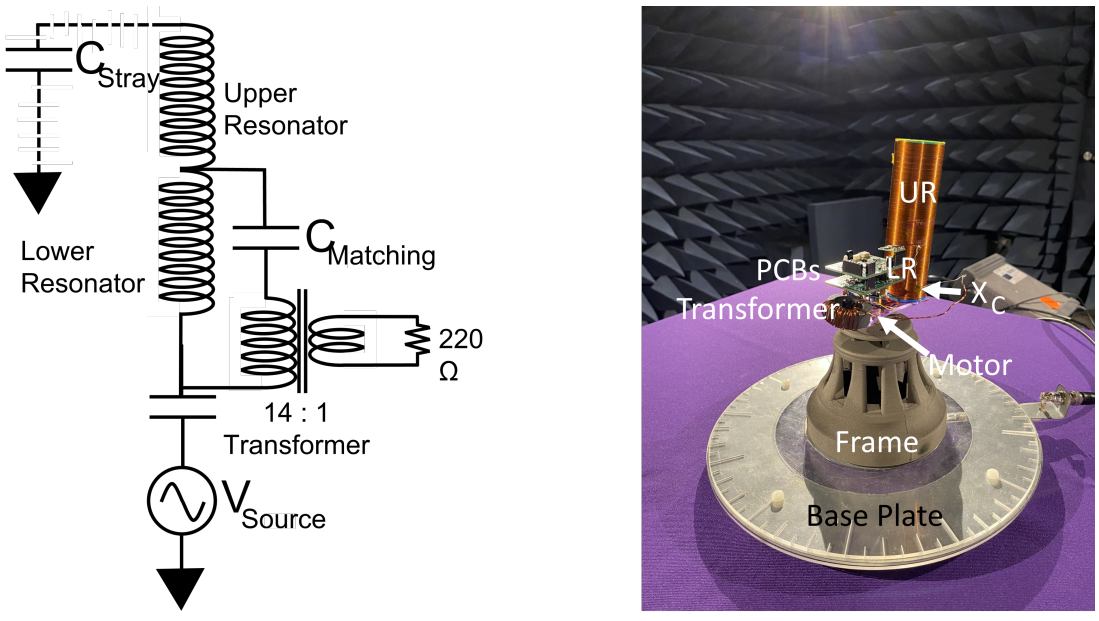

Figure 4. (**a**) A schematic of the circuit, (**b**) The robot with 1 degree of freedom functioning.

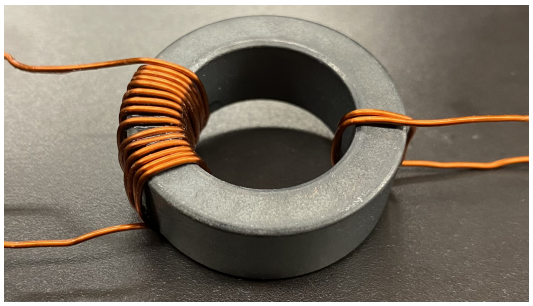

Figure 5. The transformer that is placed in parallel with the coil.

2.2. Control Scheme

The prototype load consisted of the motor with integrated control electronics. Figure 6 shows the block diagram of the motor control system. The microcontroller was an ATmega 32u4. A DRV8833PWP dual H-bridge motor driver from Texas Instruments located in Dallas, TX, USA was used to drive a brushed DC N20 motor. Figure 6 is a photograph of the fabricated control PCB. The control board used an infrared (IR) NEC communication protocol to actuate the motor left or right. The NEC protocol is advantageous as it has readily available libraries for the ATmega microcontroller and offers a low bit error rate (BER) by averaging multiple signals sent for a command. The two TSOP382 IC's receive the IR signals. A standard IR LED controller (such as found within a TV remote) was chosen as the transmitter.

A separate full bridge rectifier (Figure 7) in tandem with a 5V DC regulator was used to operate the embedded microcontroller. This was placed on a separate PCB that was positioned/stacked on top of the control board. Referring to Figure 7, the "`V_HF+`" and "`V_HF-`" are the inputs from the RF power signal that was connected to the tap/matching network of the QWR. The fabricated PCB is shown in Figure 7.

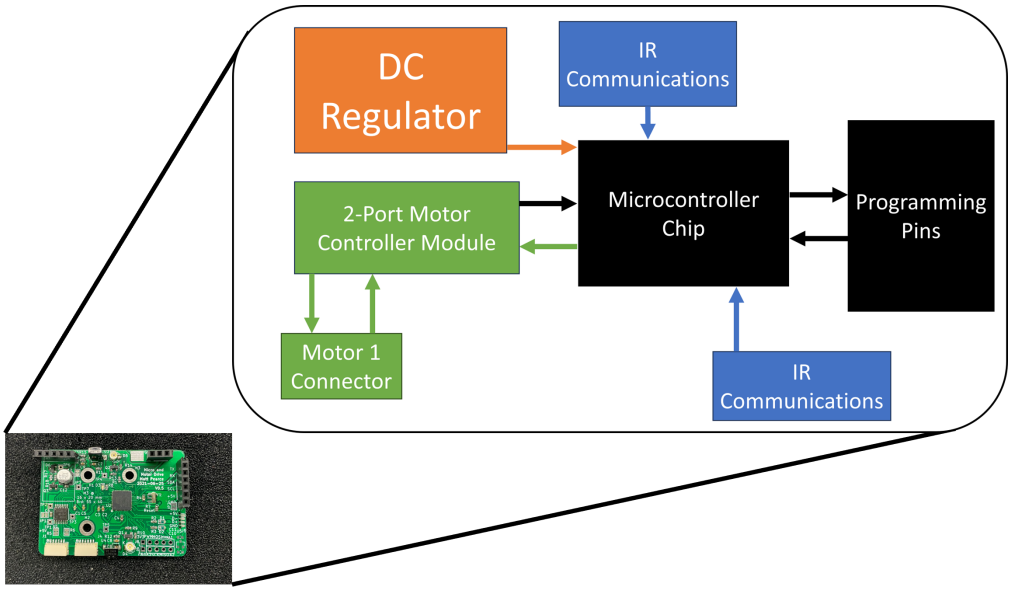

Figure 6. The block diagram for the microcontroller and motor controls with the physical microcontroller circuit board populated with the components necessary for functionality in the corner.

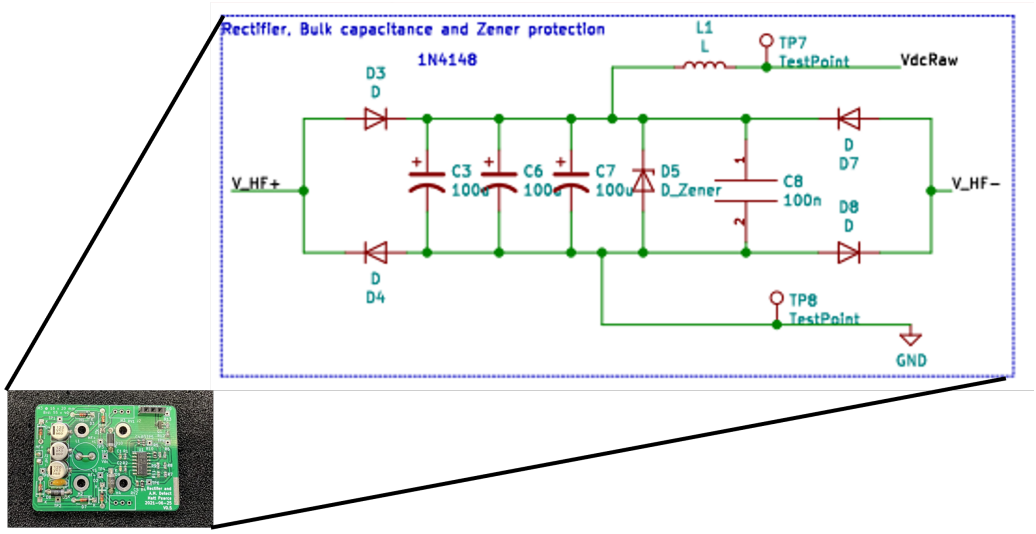

Figure 7. The schematic for the DC H-bridge rectifier with the physical AC–DC circuit board in the corner.

2.3. Unilateral Wiring Current Path

The current in the system follows a path that is along the chassis of the robot, over the motor housing/gearbox, and into the QWR. This current path will be defined as a unilateral wiring scheme, since there is no return wire anywhere in the system. Any thermal effects along the motor and associated gear box is an area of concern when being incorporated into the unilateral circuit. To investigate this, the skin depth was calculated to determine the penetration of the unilateral current flow. Using the standard equation for skin depth,

$$\delta = \sqrt{\frac{\rho}{\pi f \mu}}, \tag{24}$$

where ρ is the resistivity of the material the current flows over, f is the operating frequency, and μ is the permeability of material. Assuming the motor housing is a basic steel, μ can be estimated at approximately $1200\mu_0$ with a resistivity of 1×10^{-7} Ωm. The skin depth is on the order of 3 µm. This number is sufficient to warrant an experimental test with these motors to determine if any thermal heating occurs.

Figure 8 is a photograph of an experiment to test the heating through the motor. In this test, the motor was connected in series with an RF amplifier (The A150 RF Amplifier from Electronics and Innovation, LTD) and a QWR. This experiment was run for an hour, with 15 W being delivered to the QWR through the motor. The input current was measured at 474 mA_{RMS}. The temperature of the coil was found to be 37.72 °C and the motor was 26.29 °C. This was compared to a room temperature of 23 °C. With only a 3 degree temperature rise over the course of the 1 h, the amount of thermal heating was insignificant. Therefore, it is possible to transfer power over the motor housing and subsequent gearbox with little thermal effects due to the QWR's high-impedance operation. There are obvious limits to this approach as the system is scaled; it will become important to form capacitive links between the motor and adjacent joint. This is a focus for future work. However, the unilateral nature makes such capacitive linkages significantly easier than a bilateral CPT system. A bilateral CPT approach would require 2 transmitting plates and 2 receiving plates per linkage, increasing design complexity. The unilateral system needs only 1 transmitting plate and 1 receiving plate per linkage.

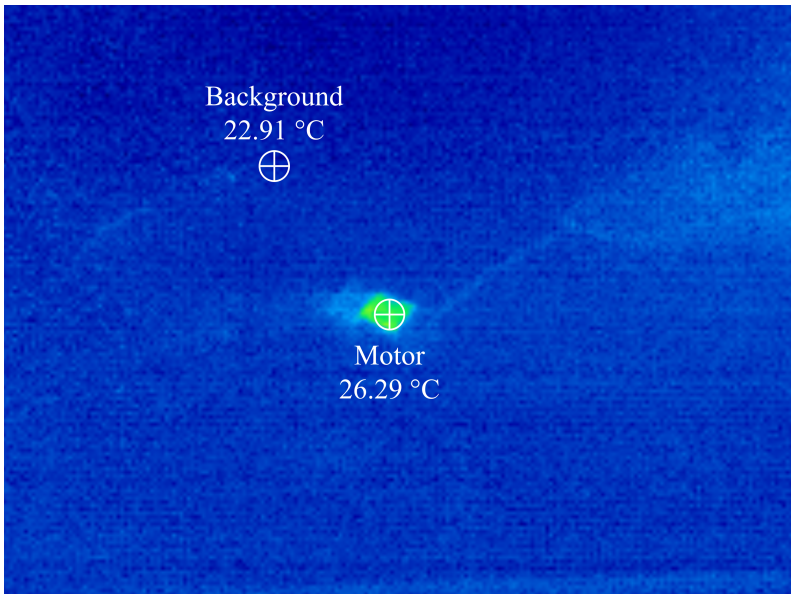

Figure 8. Thermal image investigating the power loss when using the motor housing and gearbox as part of the unilateral current path. The temperature on the motor housing rose °C above ambient after 1 h of 0.5 A passing through it at a frequency of 6.78 MHz.

3. Results

Each tap location along the QWR was tested with the matching network, as shown in Figure 4a. The QWR was maintained at its resonant frequency for every tap location tested. These changes occur due to the reduction in the electrical length of the QWR. The total system efficiency (η) was calculated by measuring the DC power output at the rectifying PCB, and dividing it by the measured AC input power at the base plate.

$$\eta = \frac{P_{Load(DC)}}{P_{in(AC)}} = \frac{V_{DC} I_{DC}}{V_{RMS} I_{RMS} \cos\theta}. \tag{25}$$

Figure 9 shows the voltage and current waveforms input to the base plate of the robotic system. From Figure 10, it can be seen that the percentage of the QWR that is tapped has a direct relationship to the efficiency. The presence of a capacitor in the load-side of the impedance branch also had a significant impact on the system transfer efficiency.

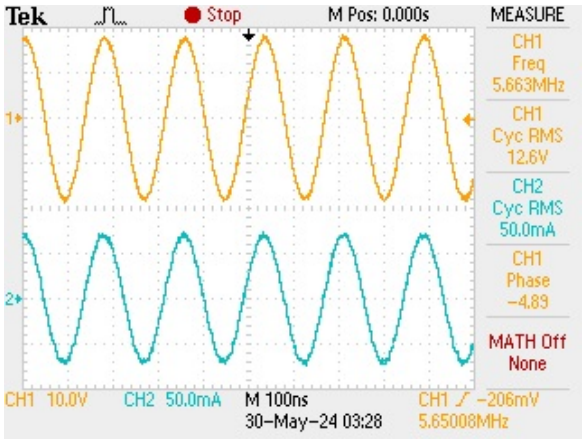

Figure 9. The input waveforms from the device used to deliver power to the robot.

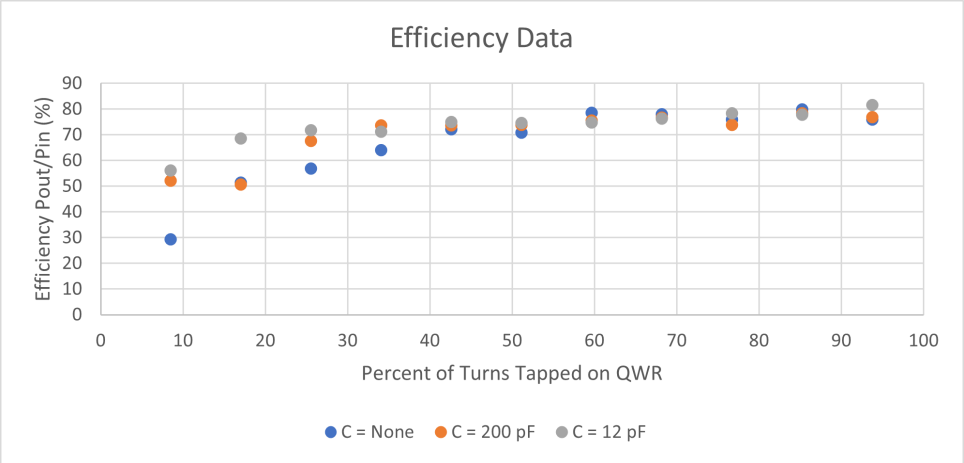

Figure 10. Graph of efficiencies.

Without any capacitance to balance the load-side branch, the efficiency was the lowest of the experimental measurements, achieving a maximum transfer efficiency of 79%. Using a capacitor to balance load-side branch, the peak efficiency of 82% was achieved. As can be seen in the figure, for all the cases tested, the efficiency reached a point where it plateaued, while the efficiency increased by a marginal amount. This plateau occurs at a tap that spans roughly 25% of the coil's length for the tests that had a matched impedance. The plateau for the test without a capacitor occurred at 43% of the coil's length (nearly half the coil). Utilizing proper matching capacitance can reduce the amount of tap size required for power transfer on the QWR. This is significant since a higher efficiency can be achieved without shifting the frequency as much. This will allow for lower frequencies to be achieved with the same QWR.

Figure 11 plots the change in the resonant frequency with tap location. The data sets for the three capacitors used show that the capacitance does not have any large bearing on the shift in frequency as more of the coil is tapped. However, the number of turns of a tap produces a linear change in the operating frequency as the tap size is increased (Figure 11). This result shows that shunting a portion of the QWR using a tap creates a reduction in the electrical length in the μcT-line. The linear response in frequency vs. tap size is beneficial for designing a QWR to operate at a desired frequency while maintaining an improved power transfer efficiency.

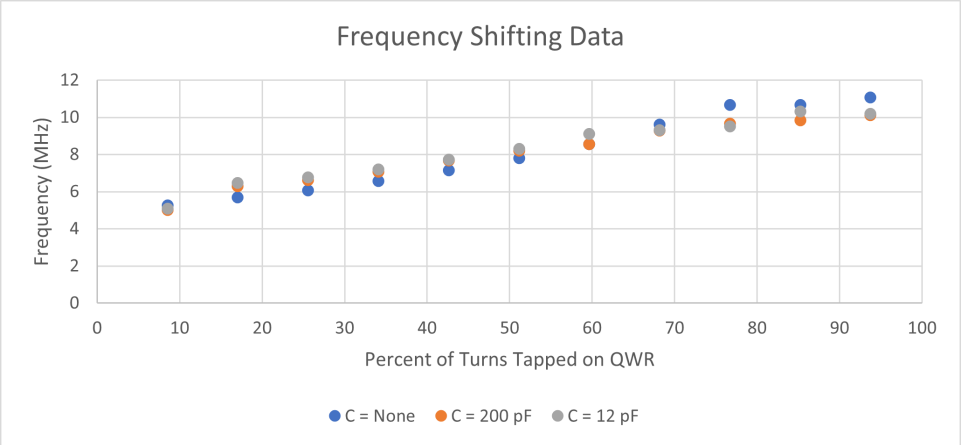

Figure 11. Graph of the effect on the resonant frequency from tapping.

The theory derived earlier in the manuscript assists in conveying what Figures 10 and 11 show, which is that this topology can be used to improve the transfer efficiency while minimally affecting the operating frequency of the system. This can be a new framework for

designing much more complex robots using impedance matching QWR topology to achieve better power transfer in the field of QWiC.

The ability to transfer power wirelessly over a robotic chassis, in a unilateral fashion, offers a unique design approach that eliminates wires between joints. Figure 12 depicts how such a unilateral wiring design can be expanded upon to operate any number of linkages using the QWiC power method. The multi-joint approach in Figure 12 is currently under development and will be communicated in a future work.

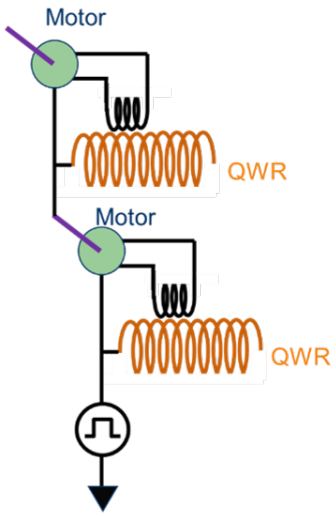

Figure 12. A future design of the robot with multiple QWRs to allow tapping to assist with all joints.

4. Discussion

A unique, unilateral current flow technique was demonstrated using a single degree of freedom to transfer power over the chassis of a robotic joint. This work explored the use of a matching capacitance in tandem with various tap locations along a QWR for improved efficiency using the single-wire QWiC method. From the efficiency data, it was determined that the tap location and matching capacitance allows one to achieve an improved power transfer scheme with a predictable effect on frequency shift of the QWR. The results from this study can be used to design a system that operates at both a specified frequency and a much higher transfer efficiency.

This novel quasi-wireless power technique opens a completely new design space, where wiring is eliminated within the chassis and between joints of machines, allowing for highly resilient systems that could have transformative impacts in robotics and their associated applications/industries.

Future work will explore different matching techniques beyond a single capacitor (such as LCC) in the load branch, along with capacitive methods of impedance transformation that do not require a transformer. Research is ongoing to improve various aspects of the design. Modulation of the RF power along the chassis could be used for communication, similar to [27].

Author Contributions: Conceptualization, T.M., C.S.J., M.P., C.P. and C.W.V.N.; Methodology, T.M., C.S.J. and C.W.V.N.; Software, T.M., J.-C.W. and M.P.; Validation, T.M., C.S.J. and C.W.V.N.; Formal analysis, T.M. and C.W.V.N.; Investigation, T.M., J.-C.W. and C.P.; Resources, C.W.V.N.; Data curation, T.M.; Writing—original draft, T.M.; Writing—review & editing, T.M., M.P., C.W.V.N., C.V. and D.B.; Visualization, J.-C.W.; Supervision, C.W.V.N.; Project administration, C.W.V.N., C.V. and D.B.; Funding acquisition, C.W.V.N. and D.B. All authors have read and agreed to the published version of the manuscript.

Funding: This research was funded by NASA Marshall Space Flight Center under Cooperative Agreement grant number 80NSSC20M0186.

Data Availability Statement: The original contributions presented in the study are included in the article, further inquiries can be directed to the corresponding author.

Acknowledgments: The research described and the resulting data presented herein this document was conducted at Tennessee Technological University with testing performed at Marshall Space Flight Center. Permission was granted by NASA to publish this information.

Conflicts of Interest: The authors declare no conflicts of interest.

References

1. Marcrum, T.; Williams, J.; Johnson, C.; Pearce, M.; Vaughan, C.; Boyd, D. Impedance Matching a Quarter Wave Resonant Receiver to Improve Efficiency in Unipolar Capacitive Wireless Power Transfer. In Proceedings of the 2023 IEEE Wireless Power Technology Conference and Expo (WPTCE), San Diego, CA, USA, 4–8 June 2023; p. 4.
2. Vital de Campos de Freitas, S.; Cezar Domingos, F.; Mirzavand, R.; Mousavi, P. Capacitive Resonant System to Charge Devices with Metallic Embodiments. In Proceedings of the 2019 IEEE Wireless Power Transfer Conference (WPTC), London, UK, 18–21 June 2019; pp. 347–350, ISSN: 2573-7651. [CrossRef]
3. Dai, J.; Ludois, D.C. A Survey of Wireless Power Transfer and a Critical Comparison of Inductive and Capacitive Coupling for Small Gap Applications. *IEEE Trans. Power Electron.* **2015**, *30*, 6017–6029. [CrossRef]
4. Wallin, T.J.; Pikul, J.; Shepherd, R.F. 3D printing of soft robotic systems. *Nat. Rev. Mater.* **2018**, *3*, 84–100. [CrossRef]
5. Slyper, R.; Hodgins, J. Prototyping robot appearance, movement, and interactions using flexible 3D printing and air pressure sensors. In Proceedings of the 2012 IEEE RO-MAN: The 21st IEEE International Symposium on Robot and Human Interactive Communication, Paris, France, 9–13 September 2012; pp. 6–11, ISSN: 1944-9437. [CrossRef]
6. Li, T.; Wang, Y.; Lang, Z.; Qi, C.; Jin, X.; Chen, X.; Xu, D. Analysis and Design of Rotary Wireless Power Transfer System with Dual-Coupled XLC/S Compensation Topology. *IEEE Trans. Ind. Appl.* **2023**, *59*, 2639–2649. [CrossRef]
7. Stuhne, D.; Hoang, V.D.; Vasiljevic, G.; Bogdan, S.; Kovacic, Z.; Ollero, A.; Ebeid, E.S.M. Design of a Wireless Drone Recharging Station and a Special Robot End Effector for Installation on a Power Line. *IEEE Access* **2022** , *10*, 88719–88737. [CrossRef]
8. Sun, Z.J.; Ye, B.; Qiu, Y.; Cheng, X.G.; Zhang, H.H.; Liu, S. Preliminary Study of a Legged Capsule Robot Actuated Wirelessly by Magnetic Torque. *IEEE Trans. Magn.* **2014**, *50*, 1–6. [CrossRef]
9. Lee, J.; Ha, J.I. Wirelessly Powered Coil-Type Robot with 1D Self-Actuation Capability. In Proceedings of the 2017 IEEE Energy Conversion Congress and Exposition (ECCE), Cincinnati, OH, USA, 1–5 October 2017; pp. 2382–2388. [CrossRef]
10. Lee, J.; Ha, J.I. Wirelessly Powered Coil-Type Robot with 2D Translational and 1D Rotational Self-Actuation Ability. In Proceedings of the 2018 15th International Conference on Ubiquitous Robots (UR), Honolulu, HI, USA, 26–30 June 2018; pp. 214–219. [CrossRef]
11. Fiorillo, F.; Beatrice, C.; Bottauscio, O.; Manzin, A.; Chiampi, M. Approach to magnetic losses and their frequency dependence in Mn–Zn ferrites. *Appl. Phys. Lett.* **2006**, *89*, 122513. [CrossRef]
12. Pasquale, M.; Fiorillo, F.; Coisson, M.; Beatrice, C. Magnetic permeability, losses and ferromagnetic resonance in ferrites under magnetic field bias from DC to the microwave regime. In Proceedings of the 2008 Conference on Precision Electromagnetic Measurements Digest, Broomfield, CO, USA, 8–13 June 2008; pp. 524–525, ISSN: 2160-0171. [CrossRef]
13. Lu, F.; Zhang, H.; Hofmann, H.; Mei, Y.; Mi, C. A dynamic capacitive power transfer system with reduced power pulsation. In Proceedings of the 2016 IEEE PELS Workshop on Emerging Technologies: Wireless Power Transfer (WoW), Knoxville, TN, USA, 4–6 October 2016; pp. 60–64. [CrossRef]
14. Muharam, A.; Mostafa, T.M.; Nugroho, A.; Hapid, A.; Hattori, R. A Single-Wire Method of Coupling Interface in Capacitive Power Transfer for Electric Vehicle Wireless Charging System. In Proceedings of the 2018 International Conference on Sustainable Energy Engineering and Application (ICSEEA), Tangerang, Indonesia, 1–2 November 2018; pp. 39–43. [CrossRef]
15. Sedehi, R.; Budgett, D.; Hu, A.P.; McCormick, D. Effects of Conductive Tissue on Capacitive Wireless Power Transfer. In Proceedings of the 2018 IEEE PELS Workshop on Emerging Technologies: Wireless Power Transfer (Wow), Montreal, QC, Canada, 3–7 June 2018; pp. 1–5. [CrossRef]
16. Funato, H.; Kobayashi, H.; Kitabayashi, T. Analysis of transfer power of capacitive power transfer system. In Proceedings of the 2013 IEEE 10th International Conference on Power Electronics and Drive Systems (PEDS), Kitakyushu, Japan, 22–25 April 2013; pp. 1015–1020, ISSN: 2164-5264. [CrossRef]
17. Lu, F.; Zhang, H.; Mi, C. A Review on the Recent Development of Capacitive Wireless Power Transfer Technology. *Energies* **2017**, *10*, 1752. [CrossRef]
18. Cheah, W.C.; Watson, S.A.; Lennox, B. Limitations of Wireless Power Transfer Technologies for Mobile Robots. *Wirel. Power Transf.* **2019**, *6*, 175–189. [CrossRef]
19. Jin, K.; Zhou, W. Wireless Laser Power Transmission: A Review of Recent Progess. *IEEE Trans. Power Electron.* **2018**, *34*, 3842–3859. [CrossRef]
20. Detka, K.; Gorecki, K. Wireless Power Transfer—A Review. *Energies* **2022**, *15*, 7236. [CrossRef]
21. Faiz, M.I.S.; Awal, M.R.; Basar, M.R.; Latiff, N.A.A.; Yahya, M.S.; Saat, S. A Comparative Review on Acoustic and Inductive Power Transfer. *J. Adv. Res. Appl. Sci. Eng. Technol.* **2025**, *44*, 188–224. [CrossRef]

22. Makhdoom, R.; Maji, S.; Sinha, S.; Etta, D.; Afridi, K. Multi-MHz In-Motion Capacitive Wireless Power Transfer System for Mobile Robots. In Proceedings of the 2022 Wireless Power Week (WPW), Bordeaux, France, 5–8 July 2022. [CrossRef]
23. Yousuf, M.A.; Das, T.K.; Khallil, M.E.; Aziz, N.A.A.; Rana, M.J.; Hossain, S. Comparison Study of Inductive Coupling and Magnetic Resonant Coupling Method for Wireless Power Transmission of Electric Vehicles. In Proceedings of the 2021 2nd International Conference on Robotics, Electrical and Signal Processing Techniques (ICREST), Dhaka, Bangladesh, 5–7 January 2021. [CrossRef]
24. Zhao, W.; Qu, X.; Lian, J.; Tse, C.K. A Family of Hybrid IPT Couplers With High Tolerance to Pad Misalignment. *IEEE Trans. Power Electron.* **2022**, *37*, 3617–3625. [CrossRef]
25. Robinson, C.A.; Pearce, M.G.S.; Lu, H.; Van Neste, C.W. Capacitive Omnidirectional Position Sensor Using a Quarter Wave Resonator. *IEEE Sens. J.* **2022**, *22*, 15817–15824. [CrossRef]
26. Van Neste, C.W.; Phani, A.; Larocque, A.; Hawk, J.E.; Kalra, R.; Banaag, M.J.; Wu, M.; Thundat, T. Quarter wavelength resonators for use in wireless capacitive power transfer. In Proceedings of the 2017 IEEE PELS Workshop on Emerging Technologies: Wireless Power Transfer (WoW), Chongqing, China, 20–22 May 2017; pp. 229–234. [CrossRef]
27. Pickering, A.K.; Hull, R.; Hawk, J.E.; Phani, A.; Neste, C.W.V.; Thundat, T. Quasi-wireless surface power and control for battery-free robotics. *Wirel. Power Transf.* **2015**, *2*, 134–142. [CrossRef]